Published

This article has original data in the JCB DataViewer
http://jcb-dataviewer.rupress.org/jcb/browse/1603

JCB: Article

Membrane expansion alleviates endoplasmic reticulum stress independently of the unfolded protein response

Sebastian Schuck,[1,2] William A. Prinz,[3] Kurt S. Thorn,[2] Christiane Voss,[3] and Peter Walter[1,2]

[1]Howard Hughes Medical Institute and [2]Department of Biochemistry and Biophysics, University of California, San Francisco, San Francisco, CA 94158
[3]Laboratory of Cell Biochemistry and Biology, National Institute of Diabetes and Digestive and Kidney Diseases, National Institutes of Health, Bethesda, MD 20892

Cells constantly adjust the sizes and shapes of their organelles according to need. In this study, we examine endoplasmic reticulum (ER) membrane expansion during the unfolded protein response (UPR) in the yeast *Saccharomyces cerevisiae*. We find that membrane expansion occurs through the generation of ER sheets, requires UPR signaling, and is driven by lipid biosynthesis. Uncoupling ER size control and the UPR reveals that membrane expansion alleviates ER stress independently of an increase in ER chaperone levels. Converting the sheets of the expanded ER into tubules by reticulon overexpression does not affect the ability of cells to cope with ER stress, showing that ER size rather than shape is the key factor. Thus, increasing ER size through membrane synthesis is an integral yet distinct part of the cellular program to overcome ER stress.

Introduction

Eukaryotic cells contain a rich variety of membrane-bound organelles. Each organelle has a unique set of functions and is distinguished by a characteristic morphology. As the need for certain cellular functions changes during growth, differentiation, or disease, cells adjust the amounts, compositions, and shapes of their organelles accordingly. To make these adjustments, cells need to be able to sense an imbalance between demand and capacity for a particular function and restore homeostasis by rearranging, synthesizing, or degrading organelle components. Molecular mechanisms underlying such homeostatic regulation have been discovered, but how they coordinate the comprehensive remodeling of entire organelles is only partially understood (Haynes et al., 2007; Ron and Walter, 2007; Sardiello et al., 2009).

The ER is a large, continuous membrane system. It is responsible for the folding of all proteins that enter the secretory pathway and is the main site of lipid biosynthesis. The ER consists of the perinuclear ER, which constitutes the nuclear envelope, and the peripheral ER, which extends throughout the cytoplasm (Voeltz et al., 2002; Borgese et al., 2006; Shibata et al., 2006). The perinuclear ER is a closed membrane sheet (or cisterna), whereas the peripheral ER is a network of sheets and tubules. Sheets are typically decorated with ribosomes, whereas tubules are mostly ribosome free. ER tubules are formed by the action of reticulon and reticulon-like proteins (Voeltz et al., 2006). These morphogenic proteins contain reticulon domains, which fold into hydrophobic hairpin structures and insert into the cytoplasmic leaflet of the ER membrane. By means of their unusual mode of membrane association and their ability to oligomerize, reticulons tubulate membranes (Hu et al., 2008; Shibata et al., 2008). Reticulons thus localize to ER tubules as they generate them. Morphogenic proteins that shape ER sheets are not known, but ribosome binding to the ER membrane may stabilize sheets (Shibata et al., 2006; Puhka et al., 2007).

ER size and shape can change dramatically (Federovitch et al., 2005; Borgese et al., 2006). Perhaps the most impressive example of the great plasticity of the ER is observed during the differentiation of B lymphocytes into plasma cells, which synthesize, fold, and secrete their own weight in antibodies every day. To cope with this enormous folding load, differentiating lymphocytes drastically increase their levels of ER chaperones (van Anken et al., 2003). Concomitantly, they massively expand their ER membrane, leading to a more than threefold

Correspondence to Sebastian Schuck: sebastian.schuck@ucsf.edu

Abbreviations used in this paper: CV, coefficient of variation; ERAD, ER-associated degradation; IE, index of expansion; UPR, unfolded protein response.

The Rockefeller University Press $30.00
J. Cell Biol. Vol. 187 No. 4 525–536
www.jcb.org/cgi/doi/10.1083/jcb.200907074

Supplemental Material can be found at:
http://jcb.rupress.org/cgi/content/full/jcb.200907074/DC1
Original image data can be found at:
http://jcb-dataviewer.rupress.org/jcb/browse/1603

increase in ER volume (Wiest et al., 1990). Similarly, induction of the ER-localized cytochrome P450 detoxification system in hepatocytes leads to a pronounced expansion of the ER membrane, which forms tightly packed whorls (Feldman et al., 1981). In more artificial settings, ectopic expression of ER transmembrane proteins in both yeast and mammalian cells frequently produces ordered arrays of unusually shaped expanded ER (Anderson et al., 1983; Wright et al., 1988; Snapp et al., 2003; Lingwood et al., 2009).

The main signaling pathway controlling ER homeostasis is the unfolded protein response (UPR), whose basic features are conserved from yeast to humans (Bernales et al., 2006a; Ron and Walter, 2007). All eukaryotes possess IRE1, which acts as a sensor for protein-folding problems in the ER; metazoans have two additional sensors, PKR-like ER kinase and ATF6. When misfolded proteins accumulate in the ER, which signals that the folding capacity of the ER is exceeded and constitutes a condition called ER stress, IRE1 is activated. In turn, IRE1 activates a transcription factor called Hac1 in yeast and XBP1 in metazoans that induces a large number of genes encoding parts of the ER-resident folding machinery. Import of these gene products into the ER augments the organelle's folding capacity. In addition, the UPR activates related functionalities such as ER-associated degradation (ERAD) and lipid biosynthesis (Cox et al., 1997; Travers et al., 2000). ERAD is responsible for the retrotranslocation of terminally misfolded proteins from the ER into the cytoplasm for proteasome-mediated degradation (Vembar and Brodsky, 2008). Without the UPR, cells cannot adjust their levels of ER chaperones according to need and are unable to maintain ER homeostasis. Knockout of IRE1 or XBP1 is lethal in mice, XBP1-deficient B lymphocytes fail to develop into plasma cells, and yeast lacking Ire1 or Hac1 are hypersensitive to ER stress (Cox et al., 1993; Mori et al., 1993, 1996; Cox and Walter, 1996; Reimold et al., 2000, 2001; Urano et al., 2000).

The role of the UPR in regulating the amount of ER membrane is less clear. Expression of active XBP1 stimulates lipid biosynthesis and enlarges the ER in fibroblasts and B lymphocytes (Shaffer et al., 2004; Sriburi et al., 2004). Conversely, XBP1 deficiency impairs the characteristic ER membrane expansion during the development of specialized secretory cells (Reimold et al., 2001; Lee et al., 2005). However, it is unknown whether removal of XBP1 abolishes the ability of these cells to expand their ER or prevents them from reaching the stage of development at which ER expansion would normally take place. In addition, experiments using UPR-deficient yeast have yielded conflicting results as to whether the UPR is needed for ER expansion upon overexpression of ER transmembrane proteins (Cox et al., 1997; Menzel et al., 1997; Takewaka et al., 1999; Larson et al., 2002). Moreover, the physiological role of ER membrane expansion has not been explored. The ER of specialized secretory cells has to process an unusually large amount of cargo, and ER stress in any cell type increases cargo load as proteins stay longer in the ER before they are correctly folded or degraded. It seems reasonable that a larger ER is needed under these circumstances to accommodate increased amounts of ER client proteins. In addition, membrane expansion during ER stress may occur concomitantly with UPR target gene activation to house newly synthesized ER-resident folding machinery. However, these notions have not been tested experimentally.

In this study, we investigate ER biogenesis in response to acute ER stress in the budding yeast *Saccharomyces cerevisiae* to address the role of UPR signaling in mediating ER membrane expansion, define the pathways involved in synthesizing new ER membrane, and gain insight into the physiological significance of the resulting increase in ER size.

Results

To visualize the yeast ER, we fluorescently labeled Sec63, an abundant ER transmembrane protein that localizes to both sheets and tubules and has been used extensively as an ER marker (Prinz et al., 2000; Voeltz et al., 2006). We generated cells in which a functional Sec63-GFP fusion protein replaced the endogenous Sec63. Optical sections through the middle of these cells showed the evenly labeled nuclear envelope and the peripheral ER, which in yeast lies just underneath the plasma membrane (Fig. 1 A, left). Peripheral and perinuclear ER are connected by a small number of tubules, which were only occasionally captured in single optical sections. In midsections, the peripheral ER appeared as a dotted line because its tubular network is seen in cross sections (Fig. 1 A, top). Its netlike morphology was more evident in cortical sections (Fig. 1 A, bottom). We estimate that ~40% of the cytoplasmic face of the plasma membrane is covered with ER (see Materials and methods).

ER stress induces ER expansion through the generation of membrane sheets

Exposure of cells to ER stress by treatment with DTT, which prevents disulfide bond formation, or tunicamycin, which inhibits protein glycosylation, caused massive ER expansion (Fig. 1 A, right). In midsections, the Sec63-GFP signal along the cell periphery had a more continuous appearance. Cortical sections showed that this reflected the generation of large membrane sheets so that the expanded peripheral ER covered ~85% of the plasma membrane. In addition, extensions of the peripheral ER into the cytoplasm were frequently seen, whereas the nuclear envelope retained its size and shape.

Using electron microscopy, we have shown previously that the membrane area of the peripheral ER (including cytoplasmic extensions) increases more than threefold during DTT treatment, whereas ER volume increases approximately fivefold (Bernales et al., 2006b). To quantify expansion of the peripheral ER from light microscopy images, we exploited the fact that Sec63-GFP, as seen in midsections, became more evenly distributed along the cell cortex as the expanding ER covered an increasing portion of the plasma membrane. We determined an index of expansion (IE) by measuring the variation of the cortical Sec63-GFP signal and normalizing it to the variation of the perinuclear Sec63-GFP signal, which represents maximally expanded ER (see Materials and methods). The resulting index does not provide an absolute measure for overall ER membrane area or volume but proved to be a sensitive and reproducible metric for the characteristic spreading of the cortical Sec63-GFP signal during ER expansion. Expansion occurred within 1 h of DTT treatment and reached

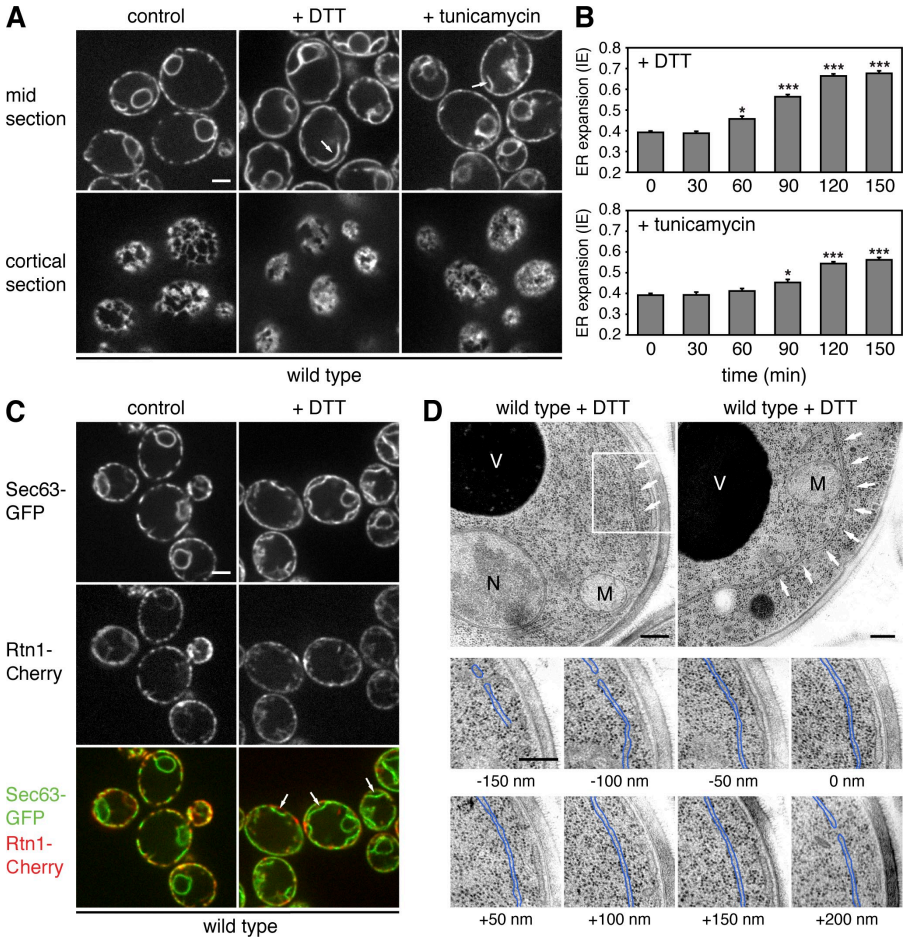

Figure 1. **ER stress induces ER membrane expansion.** (A) Sec63-GFP cells (SSY139) untreated or treated with DTT or tunicamycin for 2 h. Both ER stressors induce expansion of the peripheral ER and appearance of cytoplasmic ER extensions (arrows). (B) Quantification of ER expansion from images obtained as in A. The IE was determined as described in Materials and methods. Statistical significance compared with t = 0 of $P \leq 10^{-2}$ (*) and $P \leq 10^{-6}$ (***) is shown. Error bars indicate SEM. (C) Cytoplasmic ER extensions induced by ER stress exclude the reticulon Rtn1. Sec63-GFP Rtn1-Cherry cells (SSY421) untreated or treated with DTT for 2 h. The cytoplasmic extensions in DTT-treated cells (arrows) are almost devoid of Rtn1. (D) Cytoplasmic ER extensions induced by ER stress are large membrane sheets. Electron micrographs of wild-type cells (SSY139) treated with DTT for 2 h. (top) Low magnification images of cells with cytoplasmic ER extensions (arrows) are shown. (bottom) Sequential 50-nm sections are shown at a higher magnification corresponding to the boxed area (top). The 0-nm image is the same as that shown in the top panel. The ER membrane is traced in blue. The ER sheet shown extends for at least 350 nm in the z direction. M, mitochondrion; N, nucleus; V, vacuole. Bars: (A and C) 2 µm; (D) 250 nm.

its maximum after 2 h (Fig. 1 B and Fig. S1). Tunicamycin-induced expansion was slower and less pronounced. Because of its more rapid and stronger effects, we mostly used DTT in subsequent experiments.

To further characterize the morphology of the expanded ER, we used the reticulon Rtn1 as an additional marker. As expected, Rtn1-Cherry localized mainly to the peripheral ER in untreated cells (Fig. 1 C). After DTT treatment, Rtn1-Cherry remained associated with the peripheral ER. Notably, it was largely excluded from cytoplasmic ER extensions, suggesting that these structures are sheets. Using electron microscopy, we confirmed the expansion of peripheral ER underlying the plasma membrane (Fig. S2) and followed ribosome-studded cytoplasmic ER extensions through sequential serial sections for >300 nm and sometimes up to 800 nm (Fig. 1 D). This demonstrates that the cytoplasmic strands seen in single sections are not tubules, which are <100 nm in diameter (Voeltz et al., 2002) but part of large ER sheets. The magnitude of ER expansion suggests that it involves the synthesis of new membrane, for which we provide further evidence below (see Proper ER membrane expansion requires the Ino2/4 complex).

Proper ER membrane expansion requires UPR signaling

To determine the contribution of UPR signaling to ER membrane expansion, we analyzed *hac1* and *ire1* mutants expressing Sec63-GFP. These cells have a normal ER morphology in the absence of ER stressors (unpublished data). In contrast, DTT-induced ER membrane expansion was strongly impaired (Fig. 2 A). Quantification showed that expansion of the peripheral ER was normal up to 1 h of treatment but then stalled (Fig. 2 B). In addition, large ER patches formed in the proximity of the nucleus and at the cell periphery. Colocalization with Rtn1-Cherry and electron microscopy revealed that these patches are tangles of irregularly shaped, ribosome-free ER (Fig. 2, C and D). Given that the membrane elements in these tangles cannot be resolved by light microscopy, we could not include them in the quantification of ER membrane expansion. Therefore, it is not possible to determine quantitatively to what extent peripheral and total ER membrane amounts are reduced in DTT-treated *hac1* and *ire1* mutants. Nevertheless, the ER patches clearly show that cells cannot generate morphologically normal expanded ER without UPR signaling.

Proper ER membrane expansion requires the Ino2/4 complex

Next, we investigated the role of lipid biosynthesis in ER membrane expansion. In yeast, many phospholipid synthesis enzymes are controlled at the transcriptional level by two transcription factors, Ino2 and Ino4, which form a heterodimer and require each other to function (Ambroziak and Henry, 1994; Schwank et al., 1995). We first analyzed the expression of the Ino2/4 target gene *OPI3*, which is involved in phosphatidylcholine synthesis.

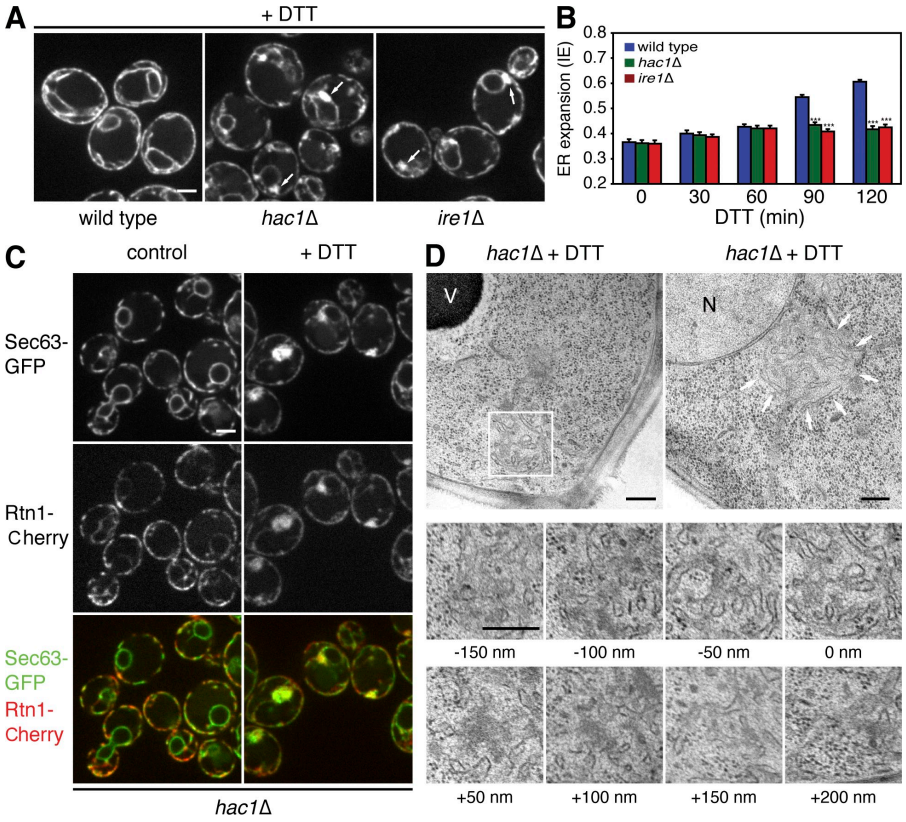

Figure 2. **Proper ER membrane expansion requires UPR signaling.** (A) Wild-type, *hac1*Δ, and *ire1*Δ cells expressing Sec63-GFP (SSY139, SSY161, and SSY467) treated with DTT for 2 h. Expansion of the peripheral ER is impaired in UPR mutants, and aberrant cytoplasmic ER patches form at the cell periphery and adjacent to the nucleus (arrows). (B) Quantification of ER expansion from images was obtained as in A. Statistical significance compared with the wild type at the same time point of $P \leq 10^{-6}$ (***) is shown. Error bars indicate SEM. (C) Sec63-GFP Rtn1-Cherry *hac1*Δ cells (SSY429) untreated or treated with DTT for 2 h. The cytoplasmic ER patches in DTT-treated cells contain both Sec63 and Rtn1. (D) Cytoplasmic ER patches induced by ER stress in *hac1*Δ cells are tangles of smooth ER. Electron micrographs of *hac1*Δ cells (SSY161) treated with DTT for 2 h. (top) Low magnification images of *hac1*Δ cells with cytoplasmic ER patches (arrows), which are found either at the cell periphery or close to the nucleus, are shown. (bottom) Sequential 50-nm sections are shown at a higher magnification corresponding to the boxed area (top). The 0-nm image is the same as shown in the top panel. The ER tangle shown consists of numerous randomly arranged ribosome-free elements. N, nucleus; V, vacuole. Bars: (A and C) 2 µm; (D) 250 nm.

DTT treatment caused a substantial induction of Opi3 protein levels (Fig. 3, A and B) in line with the previously reported induction of *OPI3* mRNA levels during the UPR (Travers et al., 2000). In contrast, the increase in Opi3 protein levels was strongly reduced in *hac1* or *ino2* mutants. The same pattern was observed for *INO1*, an Ino2/4 target gene involved in phosphatidylinositol synthesis (unpublished data). Thus, ER stress activates Ino2/4-dependent expression of lipid synthesis genes through UPR signaling. We then tested whether ER membrane expansion required the Ino2/4 complex. DTT-induced expansion was diminished in both *ino2* and *ino4* mutants, the peripheral ER retained its dotted appearance in midsections, and cytoplasmic ER extensions did not form (Fig. 3 C). In addition, aberrant ER patches were observed occasionally. Whether these are related to the patches seen in DTT-treated *hac1* and *ire1* mutants remains to be determined, but their appearance emphasized that proper ER membrane expansion fails in the absence of Ino2/4. Quantification confirmed this conclusion and additionally showed that untreated *ino2* and *ino4* mutants had a smaller ER than wild-type cells (Fig. 3 D), underscoring the role of Ino2/4 in ER size control.

If the Ino2/4 complex is important for ER membrane expansion because it regulates lipid biosynthesis, it may be possible to bypass the need for Ino2/4 by providing lipids in the growth medium. Therefore, we tested DTT-induced ER expansion of *ino2* and *ino4* mutants kept in YPD, a rich medium that includes lipids. Under this experimental regimen, ER expansion no longer required Ino2 or Ino4, and the defect in basal ER size was rescued (Fig. 3, E and F). Thus, unless lipids are supplied exogenously, full ER membrane expansion requires the Ino2/4 complex, likely because it is needed for the induction of lipid synthesis genes. In addition, these results help explain the membrane expansion defects in *hac1* and *ire1* mutants: without UPR signaling, the induction of lipid synthesis genes through activation of Ino2/4 is reduced, likely resulting in an insufficient supply of lipids to support full ER membrane expansion.

ER membrane expansion is driven by Ino2/4 activity

The identification of the Ino2/4 complex as an important player in regulating ER size enabled us to test whether activation of Ino2/4 is not only necessary but also sufficient for ER membrane expansion. When lipids are plentiful, the Ino2/4 complex is inhibited by Opi1, which binds to Ino2 (Fig. 4 A). When more lipids are needed, Opi1 dissociates from Ino2, allowing Ino2/4 to activate its target genes (Carman and Henry, 2007). To activate Ino2/4 constitutively, we either deleted *OPI1* or deleted *INO2* and provided mutant *ino2(L119A)* on a plasmid. The ino2(L119A) mutant protein cannot be bound by Opi1 and is always active (Heyken et al., 2005). Both approaches resulted in expansion of the peripheral ER (Fig. 4, B and C). The size of the nuclear envelope remained unchanged, as observed previously (O'Hara et al., 2006). ER expansion by deletion of *OPI1* required both *INO2* and *INO4*, confirming that *opi1* mutants have an expanded ER because the inhibition of Ino2/4 is relieved (Fig. S3). In addition, constitutive ER expansion in *opi1* mutants was observed in both lipid-free medium and lipid-containing YPD medium (unpublished data). Like DTT-treated wild-type cells,

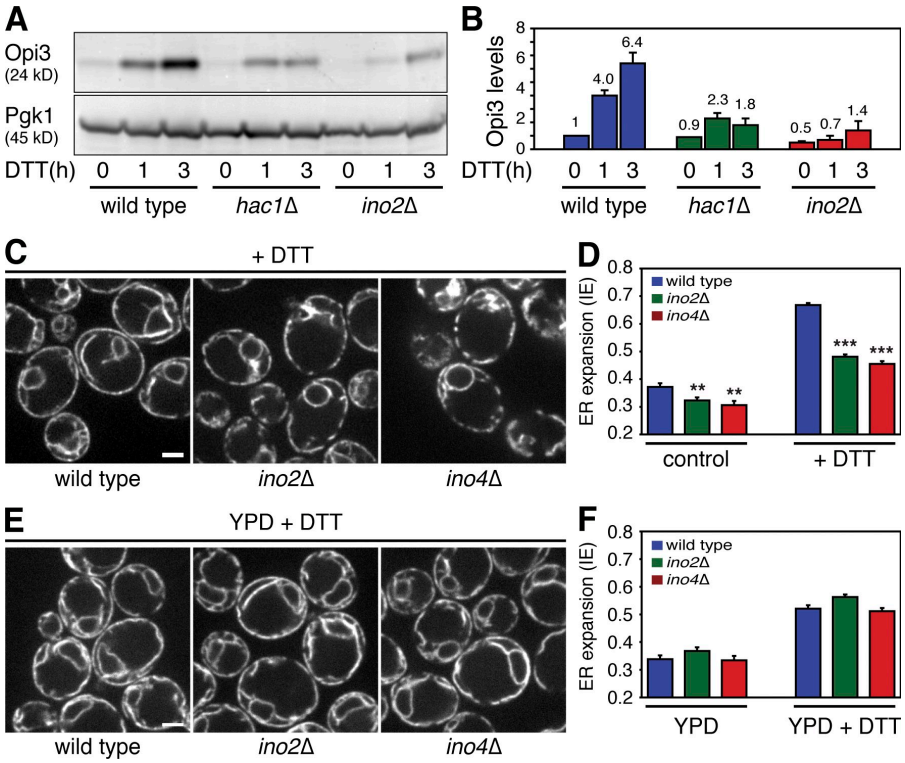

Figure 3. **Proper ER membrane expansion requires the Ino2/4 complex.** (A) ER stress increases the levels of lipid synthesis enzymes. Western blot of HA tag from Opi3-HA–expressing wild-type, *hac1*Δ, and *ino2*Δ cells (SSY477, SSY485, and SSY484) treated with DTT for up to 3 h. Pgk1 served as a loading control. (B) Quantification of Opi3 levels normalized to Pgk1 from Western blots obtained as in A. Error bars indicate SEM from three independent experiments. (C) ER expansion requires both Ino2 and Ino4. Sec63-GFP–expressing wild-type, *ino2*Δ, and *ino4*Δ cells (SSY139, SSY369, and SSY460) treated with DTT for 2 h. (D) Quantification of ER expansion from images obtained as in C. Statistical significance compared with wild-type cells of $P \leq 10^{-4}$ (**) and $P \leq 10^{-6}$ (***) is shown. Error bars indicate SEM. (E) The requirement for Ino2 and Ino4 is bypassed in lipid-containing medium. Wild-type, *ino2*Δ, and *ino4*Δ cells (SSY139, SSY369, and SSY460) treated with DTT for 2 h in YPD medium. Normal ER expansion is observed in all three strains. (F) Quantification of ER expansion from images obtained as in E. Neither *ino2*Δ nor *ino4*Δ cells show statistically significant differences compared with wild-type cells. Expansion in wild-type cells is less pronounced here because of the lower effectiveness of DTT in YPD than in SC medium. Error bars indicate SEM. Bars, 2 µm.

opi1 mutants and ino2(L119A)-expressing cells displayed ribosome-studded cytoplasmic ER extensions, which electron microscopy showed to be large ER sheets (Fig. 4 D and not depicted). These results indicate that the activation of lipid biosynthesis by Ino2/4 drives ER membrane expansion and produces an ER morphology closely resembling that generated after ER stress.

ER membrane expansion alleviates ER stress

During a normal UPR in wild-type cells, ER membrane expansion goes hand in hand with an increase in the levels of ER chaperones. Accordingly, the protein levels of the most abundant ER chaperone Kar2, the Kar2-related chaperone Lhs1, and the essential protein disulfide isomerase Pdi1 increased upon

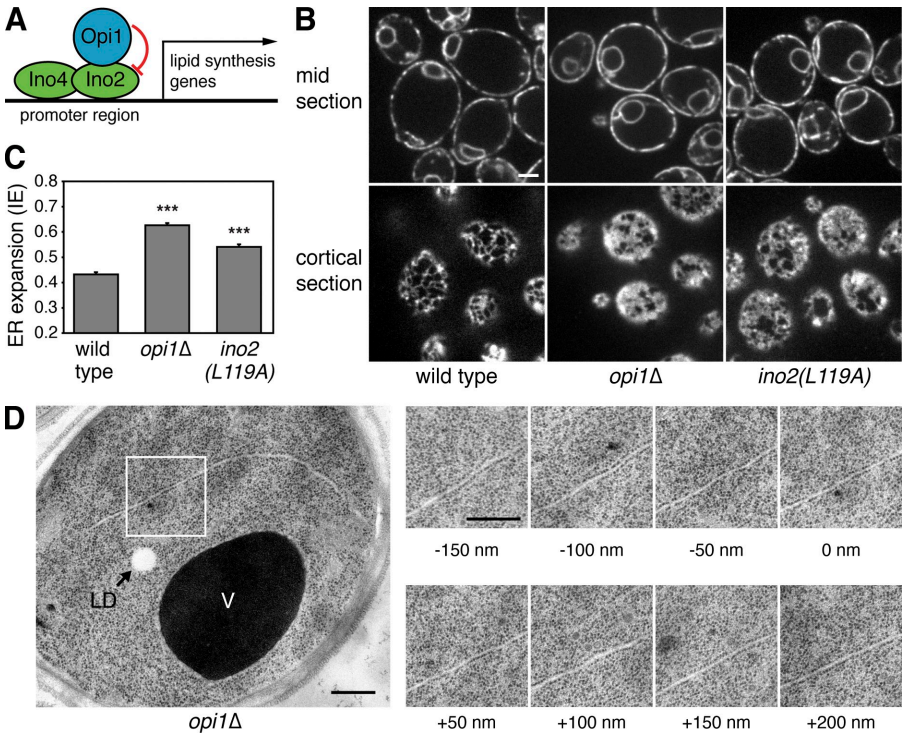

Figure 4. **ER membrane expansion is driven by Ino2/4 activity.** (A) Schematic depiction of the negative regulation of Ino2/4 by Opi1. (B) Activation of Ino2/4 results in constitutive ER expansion. Untreated wild-type, *opi1*Δ, and *ino2(L119A)* cells expressing Sec63-GFP (SSY433, SSY290, and SSY400). Bar, 2 µm. (C) Quantification of ER expansion from images obtained as in A. Statistical significance compared with wild-type cells of $P \leq 10^{-6}$ (***) is shown. Error bars indicate SEM. (D) Activation of Ino2/4 produces expanded ER morphologically similar to that generated after ER stress. Electron micrographs of untreated *opi1*Δ cells (SSY290) are shown. (left) A low magnification image is shown. (right) Sequential 50-nm sections are shown at a higher magnification corresponding to the boxed area. The 0-nm image is the same as that shown in the low magnification image. The ER sheet shown extends for at least 350 nm in the z direction. LD, lipid droplet; V, vacuole. Bars, 500 nm.

DTT treatment (Fig. 5, A and B). Strikingly, this increase was completely lacking in *OPI1*-deficient or ino2(L119A)-expressing cells (Fig. 5, C and D). Thus, these cells have a dilute ER with basal chaperone levels but an expanded ER membrane and volume. This finding shows that activation of Ino2/4 uncouples membrane expansion from an increase in ER chaperone levels. In addition, ER membrane expansion by deletion of *OPI1* or expression of ino2(L119A) still occurred in *hac1* mutants (Fig. 5, E and F), showing that membrane expansion can occur independently of UPR signaling.

The ability to experimentally uncouple ER membrane expansion and chaperone induction allowed us to address the physiological role of ER size regulation. We assessed the sensitivity of cells to ER stress by growing them on plates containing sublethal concentrations of tunicamycin for 2–3 d. For growth on plates, tunicamycin is preferable over DTT, which is quickly rendered inactive as a result of oxidation by air. To directly compare various strains with very different tunicamycin sensitivity, we chose a relatively low tunicamycin concentration that even allowed some growth of *hac1* mutants. As expected, *hac1* mutants, which cannot properly expand their ER membrane or raise their chaperone levels in response to ER stress, showed hypersensitivity to tunicamycin. *opi1* mutants were indistinguishable from wild-type cells. Revealingly, *hac1*Δ *opi1*Δ cells tolerated ER stress much better than *hac1*Δ cells (Fig. 6 A). Similarly, overexpression of Ino2 and especially Opi1-insensitive ino2(L119A) enhanced ER stress tolerance of *hac1* mutants (Fig. 6 B). These results indicate that enlarging the ER alleviates ER stress independently of an increase in chaperone levels.

If ER membrane expansion were indeed important for cells to withstand ER stress, deletion of *INO2* should render them hypersensitive to ER stressors. Consistent with this prediction, *ino2* mutants grew more slowly in the presence of tunicamycin than wild-type cells (Fig. 6 C). However, *ino2* mutants showed an obvious growth defect only at relatively high tunicamycin concentrations. An explanation for this phenotype is provided by the observation that *hac1*Δ *ino2*Δ cells already grew slowly in the absence of tunicamycin (not depicted) and were completely unable to grow at low tunicamycin concentrations (Fig. 6 D). Thus, *ino2* mutants can resist considerable ER stress with the help of the UPR but cannot overcome even mild stress when additionally deprived of *HAC1*. Furthermore, *ino2* mutants grown for an extended period of time in lipid-free medium had elevated levels of ER chaperones even in the absence of external ER stressors (Fig. 6 E). Thus, cells compensate defective ER size control after deletion of *INO2* by raising ER chaperone levels. If they are unable to do so, as in the case of *hac1*Δ *ino2*Δ cells, they become exquisitely sensitive to ER stress.

ER membrane expansion alleviates stress as a result of increased ER size rather than altered ER shape

Finally, to extend the morphological analysis of ER expansion, we sought to understand the transition from a tubular to a cisternal peripheral ER. We focused on the reticulons, which are the morphogenic proteins responsible for tubule formation. During expansion, Rtn1 retained its localization to the peripheral ER

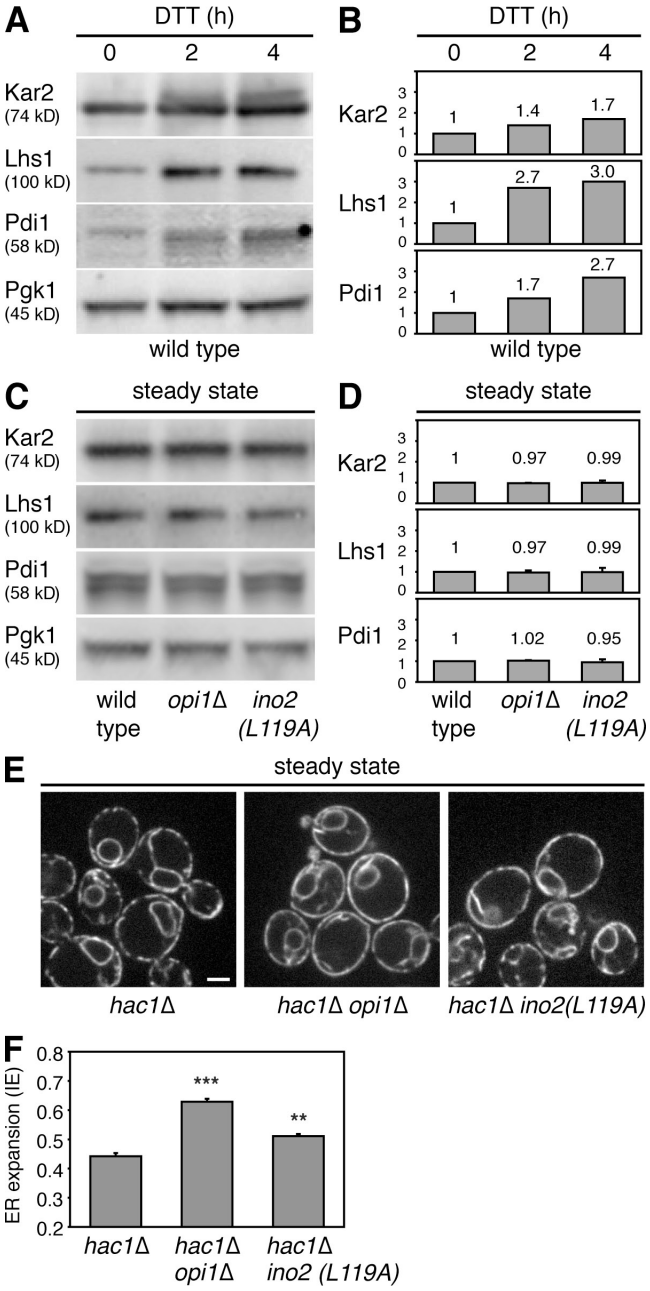

Figure 5. **ER membrane expansion can be uncoupled from the UPR.** (A) ER stress induces the levels of ER protein folding enzymes. Western blot of Kar2, Lhs1, and Pdi1 from wild-type cells (SSY139) treated with DTT for up to 4 h. Pgk1 served as a loading control. (B) Quantification of Western blotting shown in A with values normalized to Pgk1. (C) The levels of ER protein–folding enzymes are unchanged by activation of Ino2/4. Western blot of Kar2, Lhs1, and Pdi1 from untreated wild-type, *opi1*Δ, and ino2(L119A)-expressing cells (SSY433, SSY290, and SSY400). (D) Quantification of Western blots obtained as in C with values normalized to Pgk1. Error bars indicate SEM from three independent experiments. (E) ER expansion by activation of Ino2/4 can occur independently of UPR signaling. Untreated *hac1*Δ, *hac1*Δ *opi1*Δ, and *hac1*Δ *ino2(L119A)* cells expressing Sec63-GFP (SSY434, SSY364, and SSY441). Bar, 2 µm. (F) Quantification of ER expansion from images obtained as in E. Statistical significance compared with *hac1*Δ cells of $P \leq 10^{-4}$ (**) and $P \leq 10^{-6}$ (***) is shown. Error bars indicate SEM.

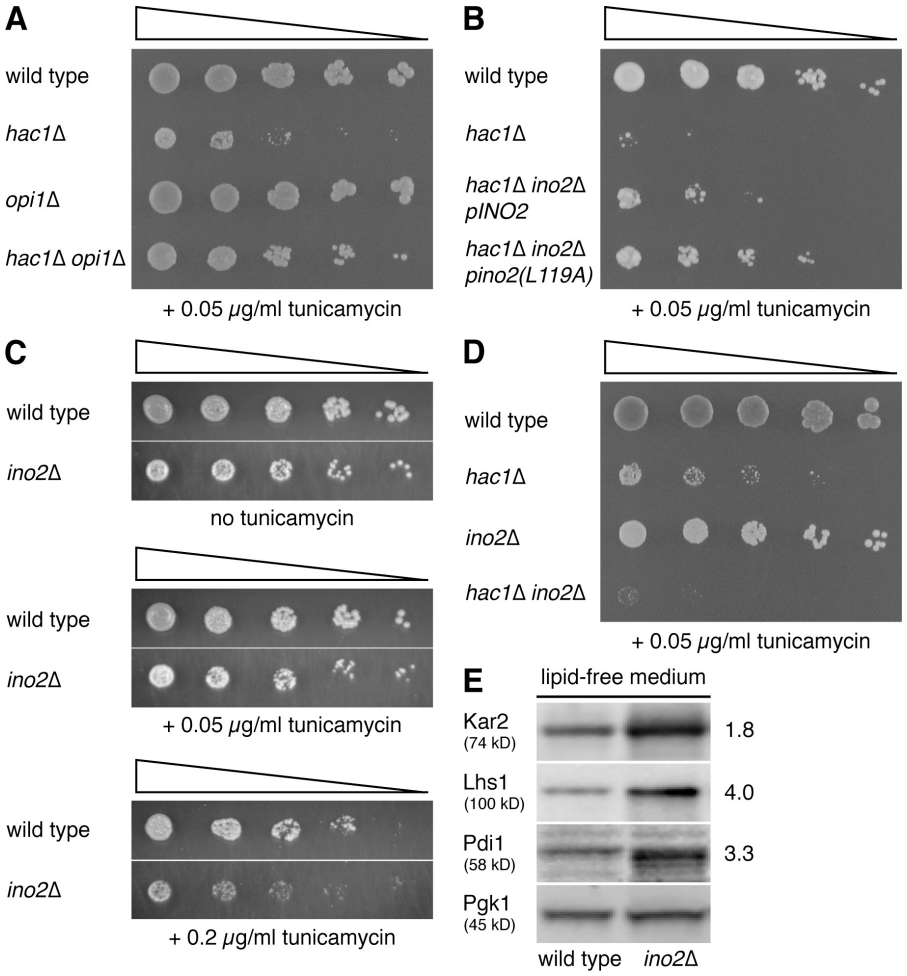

Figure 6. **ER membrane expansion alleviates ER stress.** (A) Deletion of *OPI1* increases resistance of *hac1*Δ cells to ER stress. Tunicamycin sensitivity of wild-type, *hac1*Δ, *opi1*Δ, and *hac1*Δ *opi1*Δ cells (SSY139, SSY161, SSY290, and SSY364) as assessed by plating dilution series of cells onto solid SC medium containing 0.05 μg/ml tunicamycin. Series represent fivefold dilutions from one step to the next. (B) Overexpression of Ino2 and especially ino2(L119A) increases resistance of *hac1*Δ cells to ER stress. Tunicamycin sensitivity of wild-type, *hac1*Δ, *hac1*Δ *ino2*Δ pINO2, and *hac1*Δ *ino2*Δ pino2(L119A) cells (SSY433, SSY434, SSY439, and SSY441) assessed as in A except that leucine was omitted from the plates. (C) *ino2* mutants show increased sensitivity to ER stress. Tunicamycin sensitivity of wild-type and *ino2*Δ cells (SSY139 and SSY430) assessed as in A. (D) *ino2* mutants depend on *HAC1* to overcome even mild ER stress. Tunicamycin sensitivity of wild-type, *hac1*Δ, *ino2*Δ, and *hac1*Δ *ino2*Δ cells (SSY139, SSY161, SSY369, and SSY430) assessed as in A. (E) Untreated *ino2* mutants show chaperone induction indicative of constitutive UPR signaling. Western blot of Kar2, Lhs1, and Pdi1 from untreated wild-type and *ino2*Δ cells (SSY139 and SSY369) grown for 24 h in lipid-free SC medium. Pgk1 served as a loading control. Numbers indicate fold induction in *ino2* mutants compared with wild type and normalized to Pgk1.

(Fig. 1 C). In addition, Rtn1 protein levels did not change during ER stress or upon activation of Ino2/4 (Fig. 7, A and B). This observation is consistent with earlier data showing constant mRNA levels for all three yeast reticulon and reticulon-like proteins under these conditions (Travers et al., 2000). Thus, the tubulation capacity of the reticulons may remain unchanged during ER expansion. If so, the growth of the ER membrane may overwhelm the reticulons' capacity to induce tubules, resulting in the generation of sheets. This scenario predicts that augmenting reticulon capacity should confer a tubular morphology onto the expanded ER. To test this prediction, we tagged Rtn1 with GFP to label ER tubules and additionally expressed dsRed-HDEL, which is targeted to the ER lumen and labels both tubules and sheets (Fig. 7 C, left). In *opi1* mutants, sheets were greatly expanded (Fig. 7 C, middle). Rtn1-GFP lined the sheet edges, which have a high membrane curvature. Overexpression of untagged Rtn1 in *opi1* mutants led to extensive conversion of sheets into tubules (Fig. 7 C, right). We conclude that reticulon capacity limits the amount of tubules and determines the shape of the expanded ER.

Quantification showed that the peripheral ER in *opi1* mutants remained expanded after overexpression of Rtn1 (Fig. 7 D), despite its altered shape. Thus, combining activation of Ino2/4 and reticulon overproduction uncoupled membrane expansion and sheet formation. This allowed us to further dissect the physiology of ER membrane expansion by dissociating it not only from an increase in ER chaperone levels but also from changes in ER shape. *hac1*Δ *opi1*Δ cells, which have an expanded ER but no UPR, were more resistant to tunicamycin than *hac1*Δ cells, and this increased tunicamycin resistance was unaffected by Rtn1 overexpression (Fig. 7 E). Therefore, under these conditions, ER size rather than shape was important for cells to overcome ER stress.

Discussion

Our results show that membrane expansion in response to ER stress involves the generation of large ER sheets, is restricted to the peripheral ER, and is impaired by disruption of the UPR. ER stress also induces lipid synthesis enzymes through the UPR and the Ino2/4 transcription factor complex. In the absence of Ino2/4, stress-induced membrane expansion is diminished, likely because of reduced lipid biosynthesis. Conversely, activation of Ino2/4 causes constitutive ER membrane expansion. Importantly, membrane expansion by activation of Ino2/4 occurs without a concomitant increase in ER chaperone levels and is independent of Hac1, showing that ER expansion and the UPR can be uncoupled. ER membrane expansion on its own alleviates ER stress, indicating that enlarging the ER is an integral part of an effective UPR. Furthermore, the predominantly

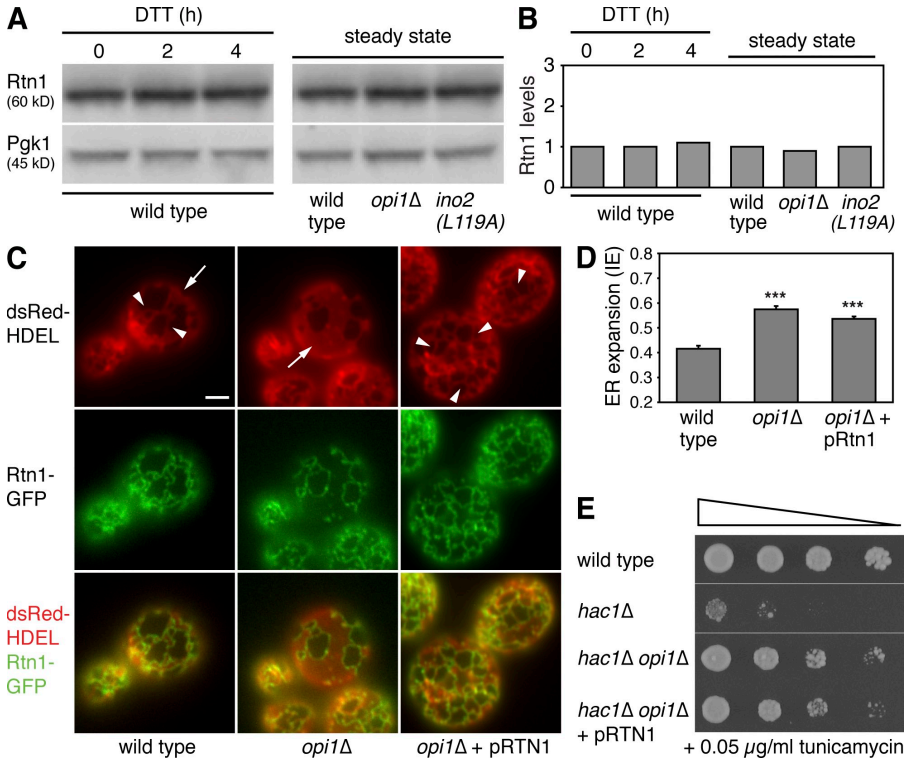

Figure 7. **ER membrane expansion alleviates stress as a result of increased ER size rather than altered ER shape.** (A) Rtn1 levels are unchanged by ER stress or activation of Ino2/4. Western blot of Cherry tag from Rtn1-Cherry–expressing wild-type cells treated with DTT for up to 4 h and from untreated Rtn1-Cherry–expressing wild-type, *opi1*Δ, and *ino2*(L119A) cells (SSY421, SSY478, and SSY473). Pgk1 served as a loading control. (B) Quantification of Western blots shown in A with values normalized to Pgk1. (C) Overexpression of Rtn1 converts sheets (arrows) into tubules (arrowheads). Untreated wild-type and *opi1*Δ cells expressing dsRed-HDEL and Rtn1-GFP were used to mark the entire ER lumen and ER tubules, respectively, and carrying an empty vector or an expression plasmid encoding untagged Rtn1 (SSY523, SSY531, and SSY532). (D) ER expansion is unaffected by Rtn1 over expression. Quantification of ER expansion from images of untreated wild-type, *opi1*Δ, and Rtn1-overexpressing *opi1*Δ cells (SSY523, SSY531, and SSY532). Statistical significance compared with wild-type cells of $P \leq 10^{-6}$ (***) is shown. Error bars indicate SEM. (E) Rtn1 overexpression does not affect sensitivity to ER stress. Tunicamycin sensitivity of wild-type, *hac1*Δ, and *hac1*Δ *opi1*Δ cells carrying empty vectors and *hac1*Δ *opi1*Δ cells carrying an expression plasmid encoding untagged Rtn1 (SSY510, SSY533, SSY535, and SSY536) as assessed by plating dilution series of cells onto solid SC medium (without uracil) containing 0.05 μg/ml tunicamycin. Series represent fivefold dilutions from one step to the next. Bar, 2 μm.

cisternal expanded ER is converted to mainly tubular by overexpression of Rtn1, suggesting that ER shape is determined by reticulon capacity. However, changing the ratio of tubules to sheets does not affect the alleviation of ER stress by membrane expansion. These findings reveal an important role of ER size control in the maintenance of ER homeostasis.

The discovery that a larger ER alone alleviates ER stress argues that the role of membrane expansion during a normal UPR, when ER size and chaperone levels increase simultaneously, goes beyond merely providing space to accommodate newly synthesized folding machinery. One possibility is that a larger ER can tolerate more misfolded proteins before essential functions break down. Moreover, a larger ER could promote protein folding itself. During folding, proteins expose hydrophobic residues that are buried in their final conformations. This makes folding intermediates vulnerable to aggregation should they encounter one another. Increasing ER volume lowers the concentration of folding intermediates, which may give proteins more time to fold by avoiding aggregate formation. This idea is consistent with in vitro experiments, showing that the unassisted folding of proteins is more efficient at low concentrations because aggregation is reduced (Apetri and Horwich, 2008). A similar mechanism might apply for membrane-associated proteins, whose dilution caused by an increase in membrane area could help avoid detrimental interactions. Finally, membrane-associated processes that support protein folding or remove misfolded proteins, such as protein glycosylation or ERAD, could operate more efficiently when a larger membrane area is available. None of these possibilities are mutually exclusive.

The observation that the shape of the expanded ER can be shifted from cisternal to tubular by simple overexpression of a reticulon suggests that ER shape depends on the balance between the amount of ER membrane and the reticulons' capacity to generate tubules. According to this view, the sheet morphology of the expanded ER during the UPR results from membrane growth without a corresponding increase in reticulon activity so that their tubulation capacity is exceeded and sheets form either by default or through the action of sheet-stabilizing proteins. A similar model invoking limiting reticulon capacity has been proposed recently to explain the formation of an appropriately sized nuclear envelope at the end of mitosis (Webster et al., 2009). We note that raising reticulon levels may only be a crude experimental substitute for how their capacity is normally regulated. Reticulon capacity could be controlled posttranslationally, perhaps by changes in oligomerization behavior (Shibata et al., 2008). The physiological significance of the transition from a tubular to a cisternal ER during the UPR remains an open question. It is not obvious whether the tubule to sheet conversion contributes to the up to fivefold increase in ER volume, and accurate measurements of the dimensions of sheets and tubules before and after ER stress by electron tomography are likely needed to answer this question. Also, it is unknown whether sheets and tubules have different functions relevant for mitigating ER stress. In any event, forcing a tubular morphology onto the expanded ER by reticulon overexpression did not affect membrane expansion or sensitivity to ER stress. Therefore, the main benefit of ER remodeling during the UPR appears to lie in the increase in ER size rather than the conversion of tubules into sheets.

The appearance of tangles of smooth tubular ER in UPR-deficient cells exposed to ER stress is intriguing. These tangles could reflect disruption of ER structure by misfolded proteins. Alternatively, they could arise from the lack of a sheet-stabilizing protein. A candidate for such a protein is Sec61, which forms the translocation channel for protein import into the ER. Sec61 is also needed for the binding of ribosomes to the ER membrane, and ribosome binding has been suggested to stabilize ER sheets (Shibata et al., 2006; Puhka et al., 2007). In addition, Sec61 is induced by ER stress in a UPR-dependent manner (Travers et al., 2000). However, *opi1* mutants and cells expressing ino2(L119A) have expanded rough ER sheets despite normal Sec61 protein levels (Fig. S4), indicating that Sec61 is not limiting for the generation of new ER sheets.

We have proposed previously that the Hac1 transcription factor coordinates the induction of chaperone genes and membrane biogenesis (Cox et al., 1997). The finding that Hac1-dependent Ino2/4 activity is needed for proper ER membrane expansion strengthens this model. In fact, the relationship between Hac1 and Ino2/4 is remarkably similar to that between the UPR and ERAD. The ERAD machinery operates at a basal level at all times but is activated during ER stress by Hac1-dependent induction of ERAD components. ERAD-deficient yeast are hypersensitive to ER stress and show constitutive activation of the UPR. Deletion of either *IRE1* or an ERAD component is tolerated well, but combined deletion causes severe synthetic phenotypes (Travers et al., 2000). Likewise, Ino2/4 activity is stimulated during ER stress through Hac1, and *ino2* mutants show increased sensitivity to tunicamycin, have elevated ER chaperone levels indicative of constitutive UPR signaling, and display synthetic sickness upon additional deletion of *HAC1*. Thus, Ino2/4 is another functional module that is recruited by Hac1 to help cells mount an effective UPR.

Nevertheless, many questions remain concerning the cascade of events that culminates in ER membrane expansion. First, it is unclear how UPR signaling activates Ino2/4-dependent transcription. A plausible mechanism is that Hac1 inhibits Opi1, thereby derepressing Ino2/4 (Cox et al., 1997; Brickner and Walter, 2004). There are several ways in which Hac1 could inhibit Opi1, e.g., by directly binding to Opi1 to promote dissociation from Ino2 or by inducing the transcription of an Opi1 inhibitor. Interestingly, Opi1 translocates from the nucleus to the peripheral ER after inositol depletion (Loewen et al., 2004) but not after DTT treatment (unpublished data), indicating different mechanisms of Ino2/4 derepression. Second, we do not know which Ino2/4 target genes are critical for ER membrane expansion. Given that the requirement for Ino2/4 is bypassed when lipids are provided exogenously, lipid synthesis genes are probably a key. We tested several Ino2/4-regulated lipid synthesis genes, including *INO1*, *PSD1*, *CHO2*, and *OPI3*, but no single deletion phenocopied the ER expansion defect seen in *ino2* and *ino4* mutants (unpublished data). Third, it remains to be determined whether deletions of *INO2* and *INO4* are truly equivalent. It is generally accepted that neither transcription factor can function without the other, but some gene promoters appear to be bound by only one of the two proteins (Lee et al., 2002), and a previous study concluded that membrane proliferation after expression of the canine ribosome receptor in yeast required *INO2* but not *INO4* (Block-Alper et al., 2002). Fourth, the residual expansion seen in *hac1* and *ire1* mutants and the residual increase in Opi3 and Ino1 protein levels in *HAC1*-deficient cells suggest that another signaling pathway exists in yeast that can sense ER stress and induce membrane expansion. This putative second pathway, which may correspond to the recently described super–UPR pathway (Leber et al., 2004), could also help explain why overexpression of ER transmembrane proteins can still trigger ER expansion in *IRE1*-deficient yeast (Menzel et al., 1997; Larson et al., 2002). Perhaps this alternative pathway is sufficient to allow long-term adaptation of ER size but is overwhelmed by the acute ER stress caused by DTT or tunicamycin. Finally, it is intriguing that the size of the nuclear envelope does not change during UPR. Unlike mammalian cells, yeast do not have nuclear lamins that could act as a scaffold to restrict nuclear size during ER membrane expansion. However, it has been found that at least part of the yeast nuclear envelope can resist expansion by an unknown mechanism (Campbell et al., 2006).

Similar to yeast, full ER expansion in mammals requires the Hac1 homologue XBP1, but some residual expansion still seems possible in its absence (Lee et al. 2005). This points to additional signaling pathways that can regulate ER size, and the ATF6 pathway has recently been suggested to play such a role (Bommiasamy et al., 2009). Also, similar to yeast, UPR signaling activates lipid biosynthesis in fibroblasts, and experimentally activating phosphatidylcholine synthesis leads to ER membrane expansion without an accompanying increase in ER chaperone levels (Sriburi et al., 2004, 2007). Although the expansion elicited by increased phosphatidylcholine production was modest compared with that achieved by expression of active XBP1, these results indicate that ER membrane expansion may be driven by lipid biosynthesis also in mammalian cells. Because there is no known mammalian master regulator of lipid biosynthesis analogous to the yeast Ino2/4 complex, it is difficult to test whether a more comprehensive activation of lipid biosynthesis would recapitulate UPR-mediated ER membrane expansion, as is the case in yeast. Nevertheless, it would be interesting to further explore the poorly understood regulation of mammalian lipid biosynthesis by the UPR (Acosta-Alvear et al., 2007).

In summary, ER stress induces membrane expansion through UPR-mediated activation of lipid biosynthesis, and the subsequent increase in ER size on its own is sufficient to alleviate stress. Thus, the UPR maintains ER homeostasis by two intimately connected but distinct mechanisms: by providing new ER-folding machinery and by providing more ER surface area and lumenal space.

Materials and methods

Antibodies and plasmids

The following primary antibodies were used: mouse anti-HA (Covance), mouse anti-Pgk1 (Invitrogen), rabbit anti-Kar2 (Walter laboratory, University of California, San Francisco, San Francisco, CA), sheep anti-Lhs1 (provided by C.J. Stirling, University of Manchester, Manchester, England, UK; Tyson and Stirling, 2000), rabbit anti-Pdi1 (provided by J. Winther, Carlsberg Laboratory, Copenhagen, Denmark), rabbit anti-dsRed (MBL International), and rabbit anti-Sec61 (Walter laboratory). Secondary antibodies conjugated to alkaline phosphatase were obtained from Millipore. Centromeric expression plasmids pRS415-MET25-INO2

and pRS415-MET25-ino2(L119A) (Heyken et al., 2005), which are derived from pRS415-MET25 (Mumberg et al., 1994), were provided by H.J. Schüller (Institut für Genetik und Funktionelle Genomforschung, Greifswald, Germany). The integrative expression plasmid YIplac-dsRED-HDEL-NatMX (Madrid et al., 2006) was provided by K. Weiss (University of California, Berkeley, Berkeley, CA) and encodes dsRed-HDEL that is targeted to the ER lumen by a signal sequence and retained there by an HDEL sequence. To make the multicopy expression plasmid YEplac195-RTN1, which encodes Rtn1 controlled by its own promoter, the coding sequence of *RTN1* plus 400 bps upstream of the start was amplified by PCR from chromosomal DNA and cloned into YEplac195 (Gietz and Sugino, 1988) between the SphI and KpnI sites.

Yeast strains

All strains used were generated in this study, derived from a W303 wild-type strain (*MATa; leu2-3,112; trp1-1; can1-100; ura3-1; ade2-1; his3-11,15*), are listed in Table S1. Gene deletions and modifications were introduced by a PCR-based method (Longtine et al., 1998). Strains expressing dsRed-HDEL were created by transformation with EcoRV-linearized YIPlac-dsRED-HDEL-NatMX. Tagging the essential Sec63 protein with GFP did not affect cell growth, indicating that the Sec63-GFP fusion protein was functional.

Light microscopy

Strains without plasmids were grown at 30°C in YPD medium unless indicated otherwise. When cultures had reached early log phase (OD_{600} = 0.15 − 0.2), cells were washed with 1 vol of SC medium (containing yeast nitrogen base, amino acids, and 2% dextrose) and resuspended in the same volume of fresh SC. The only exception to this switch from lipid-containing YPD to lipid-free SC was the experiment shown in Fig. 3 E, in which cells were washed and resuspended in fresh YPD. Strains carrying plasmids were grown, washed, and resuspended in SC without leucine or uracil as appropriate. Cells were left untreated or treated with 8 mM DTT (Roche) or 1 µg/ml tunicamycin (EMD) for the times indicated. Cells from 1 ml culture were pelleted at 10,000 *g* for 1.5 min and resuspended in ∼30 µl SC. 7 µl was transferred onto a glass slide, covered with a 22 × 50–mm cover glass, and immediately imaged live at room temperature. Images with an optical thickness of ∼700 nm were acquired on a spinning-disk confocal microscope (provided by the Nikon Imaging Center, University of California, San Francisco) consisting of an inverted microscope (TE2000U; Nikon), a spinning-disk confocal microscope (CSU22; Yokogawa), a camera (Cascade II:512; Photometrics), and a Plan Apo VC 100×/1.4 NA oil objective lens (Nikon), and was controlled by the MicroManager program (Stuurman et al., 2007). GFP was excited at 488 nm with an argon laser and imaged using a 525/50 emission filter. Cherry was excited at 568 nm with an argon krypton laser and imaged using a 615/55 emission filter. For the experiment shown in Fig. 7 C, a widefield microscope (BX61; Olympus), a UPlan Apo 100×/1.35 NA oil objective lens, a camera (Retiga EX; QImaging), and the iVision program (BioVision, Inc.) were used. The brightness and contrast of the resulting images was adjusted using Photoshop (Adobe).

Image analysis

To estimate the coverage of the plasma membrane with ER, unprocessed 16-bit image files of cortical sections were analyzed using MatLab (MathWorks). A region of interest was defined for at least 15 cells per condition, and using an identical threshold for all images, the fraction of pixels with Sec63-GFP signal was determined. To quantify ER expansion without selecting regions of interest or thresholding, optical sections through the middle of yeast cells were used. Using a modified version of an existing script for the quantification of plasma membrane signal (provided by E. Marco, Harvard Medical School, Boston, MA; Marco et al., 2007), we first determined the intensity of the Sec63-GFP signal along the cell cortex. We calculated the intensity's coefficient of variation (CV), i.e., the standard deviation of the intensity divided by its mean. Untreated wild-type cells gave high CV values as a result of the large fluctuations of the cortical Sec63-GFP signal, which resulted from the dotted appearance of the cross sectioned tubular ER network. Cells with expanded ER yielded lower CV values as Sec63-GFP became more evenly distributed along the cortex within large ER sheets. To calculate the IE of the peripheral ER, we made use of the fact that the perinuclear Sec63-GFP signal, which represents the closed membrane sheet that makes up the nuclear envelope, sets the value for maximally expanded ER and gives the lowest possible CV. We defined IE as the CV for nuclear envelope of untreated wild-type cells divided by the CV for cortical signal of cells of interest so that ER expansion resulted in an increase of IE. The IE is not as intuitive as estimates of the coverage of the plasma membrane with ER but has several advantages. It is very reproducible, can be obtained without image manipulation of any kind, and can be calculated from midsections, which are easier to acquire than well-focused cortical sections. 30–40 cells were quantified per condition, the mean of IE ± SEM was determined, and Student's *t* test was used to assess statistical significance of differences between conditions. The MatLab script we used is provided in the Online supplemental material.

Electron microscopy

Cells were grown to early log phase at 30°C in 100 ml YPD, washed with SC, and resuspended in 100 ml fresh SC. Cells were left untreated or treated with 8 mM DTT for 2 h and processed essentially as described previously (McDonald and Müller-Reichert, 2002; Bernales et al., 2006b). In brief, cells were filtered and rapidly frozen using a high pressure freezer (EM PACT; Leica). Samples were transferred onto frozen fixative (1% osmium tetroxide, 0.1% uranyl acetate, and 3% water in acetone), freeze substituted with a freeze substitution system (EM AFS2; Leica), and embedded in epon resin. 50-nm-thin sections were cut, stained with 2% aqueous uranyl acetate for 3 min and Reynold's lead citrate for 1 min, and viewed under an electron microscope (Tecnai 12; FEI).

Western blotting

Cells were grown at 30°C in YPD or SC lacking leucine to maintain plasmid selection where appropriate. Where indicated, cells were treated with DTT as described in the previous paragraph. For the experiment shown in Fig. 6 E, cells were grown in YPD, washed, switched to SC, and grown for another 24 h. Cells were harvested by centrifugation, washed twice with water to remove DTT that would interfere with the subsequent protein determination, and were disrupted by bead beating. Proteins were extracted with urea and SDS, and protein concentrations were measured using the bicinchoninic acid protein assay kit (Thermo Fisher Scientific). 10–50 µg total protein was resolved on Bis-Tris gels (NuPAGE; Invitrogen) and transferred onto polyvinylidene difluoride membranes. Membranes were blocked, probed with primary and secondary antibodies, and incubated with enhanced chemifluorescence substrate (GE Healthcare). Fluorescence was detected with a variable mode imager (Typhoon 9400; GE Healthcare) and quantified using ImageQuant (GE Healthcare).

Growth assay

Cells were grown at 30°C in YPD or SC lacking leucine or uracil until they had reached log phase (OD_{600} = 0.2–0.4). Cultures were diluted to 2.5 × 10^6 cells/ml, dilution series with fivefold dilution steps were prepared, and 2 µl of each dilution, i.e., 5 × 10^3 cells at the highest concentration, were spotted onto SC plates containing the indicated concentrations of tunicamycin. Plates were incubated at 30°C for 2–3 d.

Online supplemental material

Fig. S1 shows Sec63-GFP expressing wild-type cells treated with DTT for up to 150 min. Fig. S2 shows electron micrographs of untreated and DTT-treated wild-type cells. Fig. S3 shows Sec63-GFP expressing *opi1*Δ, *opi1*Δ *ino2*Δ, and *opi1*Δ *ino4*Δ cells. Fig. S4 shows Sec61 protein levels of untreated and DTT-treated wild-type and *hac1*Δ cells and of untreated *opi1*Δ and *ino2(L119A)* cells. Table S1 lists all of the yeast strains used in this study. The MatLab script used for image analysis is also provided. Online supplemental material is available at http://www.jcb.org/cgi/content/full/jcb.200907074/DC1.

We thank Colin Stirling and Jacob Winther for antibodies, Hans-Joachim Schüller and Karsten Weiss for plasmids, and Eugenio Marco for the MatLab script. We are grateful to Kent McDonald and Mei Lie Wong for help and advice on electron microscopy, to Diego Acosta Alvear, Georg Borner, Brooke Gardner, Benoit Kornmann, Han Li, Saskia Neher, Anne-Lore Schlaitz, and Eelco van Anken for comments on the manuscript, and to all members of the Walter laboratory, especially Tomas Aragon and Benoit Kornmann, for discussion and ideas.

S. Schuck was supported by the Ernst Schering Foundation and the International Human Frontier Science Program Organization, W.A. Prinz and C. Voss were supported by the Intramural Research Program of the National Institute of Diabetes and Digestive and Kidney Diseases, and P. Walter is an Investigator of the Howard Hughes Medical Institute.

Submitted: 14 July 2009
Accepted: 19 October 2009

References

Acosta-Alvear, D., Y. Zhou, A. Blais, M. Tsikitis, N.H. Lents, C. Arias, C.J. Lennon, Y. Kluger, and B.D. Dynlacht. 2007. XBP1 controls diverse cell type- and condition-specific transcriptional regulatory networks. *Mol. Cell.* 27:53–66. doi:10.1016/j.molcel.2007.06.011

Ambroziak, J., and S.A. Henry. 1994. INO2 and INO4 gene products, positive regulators of phospholipid biosynthesis in *Saccharomyces cerevisiae*, form a complex that binds to the INO1 promoter. *J. Biol. Chem.* 269:15344–15349.

Anderson, R.G., L. Orci, M.S. Brown, L.M. Garcia-Segura, and J.L. Goldstein. 1983. Ultrastructural analysis of crystalloid endoplasmic reticulum in UT-1 cells and its disappearance in response to cholesterol. *J. Cell Sci.* 63:1–20.

Apetri, A.C., and A.L. Horwich. 2008. Chaperonin chamber accelerates protein folding through passive action of preventing aggregation. *Proc. Natl. Acad. Sci. USA.* 105:17351–17355. doi:10.1073/pnas.0809794105

Bernales, S., F.R. Papa, and P. Walter. 2006a. Intracellular signaling by the unfolded protein response. *Annu. Rev. Cell Dev. Biol.* 22:487–508. doi:10.1146/annurev.cellbio.21.122303.120200

Bernales, S., K.L. McDonald, and P. Walter. 2006b. Autophagy counterbalances endoplasmic reticulum expansion during the unfolded protein response. *PLoS Biol.* 4:e423.

Block-Alper, L., P. Webster, X. Zhou, L. Supeková, W.H. Wong, P.G. Schultz, and D.I. Meyer. 2002. IN02, a positive regulator of lipid biosynthesis, is essential for the formation of inducible membranes in yeast. *Mol. Biol. Cell.* 13:40–51.

Bommiasamy, H., S.H. Back, P. Fagone, K. Lee, S. Meshinchi, E. Vink, R. Sriburi, M. Frank, S. Jackowski, R.J. Kaufman, and J.W. Brewer. 2009. ATF6alpha induces XBP1-independent expansion of the endoplasmic reticulum. *J. Cell Sci.* 122:1626–1636. doi:10.1242/jcs.045625

Borgese, N., M. Francolini, and E. Snapp. 2006. Endoplasmic reticulum architecture: structures in flux. *Curr. Opin. Cell Biol.* 18:358–364. doi:10.1016/j.ceb.2006.06.008

Brickner, J.H., and P. Walter. 2004. Gene recruitment of the activated INO1 locus to the nuclear membrane. *PLoS Biol.* 2:e342. doi:10.1371/journal.pbio.0020342

Campbell, J.L., A. Lorenz, K.L. Witkin, T. Hays, J. Loidl, and O. Cohen-Fix. 2006. Yeast nuclear envelope subdomains with distinct abilities to resist membrane expansion. *Mol. Biol. Cell.* 17:1768–1778. doi:10.1091/mbc.E05-09-0839

Carman, G.M., and S.A. Henry. 2007. Phosphatidic acid plays a central role in the transcriptional regulation of glycerophospholipid synthesis in *Saccharomyces cerevisiae*. *J. Biol. Chem.* 282:37293–37297. doi:10.1074/jbc.R700038200

Cox, J.S., and P. Walter. 1996. A novel mechanism for regulating activity of a transcription factor that controls the unfolded protein response. *Cell.* 87:391–404. doi:10.1016/S0092-8674(00)81360-4

Cox, J.S., C.E. Shamu, and P. Walter. 1993. Transcriptional induction of genes encoding endoplasmic reticulum resident proteins requires a transmembrane protein kinase. *Cell.* 73:1197–1206. doi:10.1016/0092-8674(93)90648-A

Cox, J.S., R.E. Chapman, and P. Walter. 1997. The unfolded protein response coordinates the production of endoplasmic reticulum protein and endoplasmic reticulum membrane. *Mol. Biol. Cell.* 8:1805–1814.

Federovitch, C.M., D. Ron, and R.Y. Hampton. 2005. The dynamic ER: experimental approaches and current questions. *Curr. Opin. Cell Biol.* 17:409–414. doi:10.1016/j.ceb.2005.06.010

Feldman, D., R.L. Swarm, and J. Becker. 1981. Ultrastructural study of rat liver and liver neoplasms after long-term treatment with phenobarbital. *Cancer Res.* 41:2151–2162.

Gietz, R.D., and A. Sugino. 1988. New yeast-*Escherichia coli* shuttle vectors constructed with in vitro mutagenized yeast genes lacking six-base pair restriction sites. *Gene.* 74:527–534. doi:10.1016/0378-1119(88)90185-0

Haynes, C.M., K. Petrova, C. Benedetti, Y. Yang, and D. Ron. 2007. ClpP mediates activation of a mitochondrial unfolded protein response in *C. elegans*. *Dev. Cell.* 13:467–480. doi:10.1016/j.devcel.2007.07.016

Heyken, W.T., A. Repenning, J. Kumme, and H.J. Schüller. 2005. Constitutive expression of yeast phospholipid biosynthetic genes by variants of Ino2 activator defective for interaction with Opi1 repressor. *Mol. Microbiol.* 56:696–707. doi:10.1111/j.1365-2958.2004.04499.x

Hu, J., Y. Shibata, C. Voss, T. Shemesh, Z. Li, M. Coughlin, M.M. Kozlov, T.A. Rapoport, and W.A. Prinz. 2008. Membrane proteins of the endoplasmic reticulum induce high-curvature tubules. *Science.* 319:1247–1250. doi:10.1126/science.1153634

Larson, L.L., M.L. Parrish, A.J. Koning, and R.L. Wright. 2002. Proliferation of the endoplasmic reticulum occurs normally in cells that lack a functional unfolded protein response. *Yeast.* 19:373–392. doi:10.1002/yea.839

Leber, J.H., S. Bernales, and P. Walter. 2004. IRE1-independent gain control of the unfolded protein response. *PLoS Biol.* 2:E235. doi:10.1371/journal.pbio.0020235

Lee, T.I., N.J. Rinaldi, F. Robert, D.T. Odom, Z. Bar-Joseph, G.K. Gerber, N.M. Hannett, C.T. Harbison, C.M. Thompson, I. Simon, et al. 2002. Transcriptional regulatory networks in *Saccharomyces cerevisiae*. *Science.* 298:799–804. doi:10.1126/science.1075090

Lee, A.H., G.C. Chu, N.N. Iwakoshi, and L.H. Glimcher. 2005. XBP-1 is required for biogenesis of cellular secretory machinery of exocrine glands. *EMBO J.* 24:4368–4380. doi:10.1038/sj.emboj.7600903

Lingwood, D., S. Schuck, C. Ferguson, M.J. Gerl, and K. Simons. 2009. Generation of cubic membranes by controlled homotypic interaction of membrane proteins in the endoplasmic reticulum. *J. Biol. Chem.* 284:12041–12048. doi:10.1074/jbc.M900220200

Loewen, C.J., M.L. Gaspar, S.A. Jesch, C. Delon, N.T. Ktistakis, S.A. Henry, and T.P. Levine. 2004. Phospholipid metabolism regulated by a transcription factor sensing phosphatidic acid. *Science.* 304:1644–1647. doi:10.1126/science.1096083

Longtine, M.S., A. McKenzie III, D.J. Demarini, N.G. Shah, A. Wach, A. Brachat, P. Philippsen, and J.R. Pringle. 1998. Additional modules for versatile and economical PCR-based gene deletion and modification in *Saccharomyces cerevisiae*. *Yeast.* 14:953–961. doi:10.1002/(SICI)1097-0061(199807)14:10<953::AID-YEA293>3.0.CO;2-U

Madrid, A.S., J. Mancuso, W.Z. Cande, and K. Weis. 2006. The role of the integral membrane nucleoporins Ndc1p and Pom152p in nuclear pore complex assembly and function. *J. Cell Biol.* 173:361–371. doi:10.1083/jcb.200506199

Marco, E., R. Wedlich-Soldner, R. Li, S.J. Altschuler, and L.F. Wu. 2007. Endocytosis optimizes the dynamic localization of membrane proteins that regulate cortical polarity. *Cell.* 129:411–422. doi:10.1016/j.cell.2007.02.043

McDonald, K., and T. Müller-Reichert. 2002. Cryomethods for thin section electron microscopy. *Methods Enzymol.* 351:96–123.

Menzel, R., F. Vogel, E. Kärgel, and W.H. Schunck. 1997. Inducible membranes in yeast: relation to the unfolded-protein-response pathway. *Yeast.* 13:1211–1229. doi:10.1002/(SICI)1097-0061(199710)13:13<1211::AID-YEA168>3.0.CO;2-8

Mori, K., W. Ma, M.J. Gething, and J. Sambrook. 1993. A transmembrane protein with a cdc2+/CDC28-related kinase activity is required for signaling from the ER to the nucleus. *Cell.* 74:743–756. doi:10.1016/0092-8674(93)90521-Q

Mori, K., T. Kawahara, H. Yoshida, H. Yanagi, and T. Yura. 1996. Signalling from endoplasmic reticulum to nucleus: transcription factor with a basic-leucine zipper motif is required for the unfolded protein-response pathway. *Genes Cells.* 1:803–817. doi:10.1046/j.1365-2443.1996.d01-274.x

Mumberg, D., R. Müller, and M. Funk. 1994. Regulatable promoters of *Saccharomyces cerevisiae*: comparison of transcriptional activity and their use for heterologous expression. *Nucleic Acids Res.* 22:5767–5768. doi:10.1093/nar/22.25.5767

O'Hara, L., G.S. Han, S. Peak-Chew, N. Grimsey, G.M. Carman, and S. Siniossoglou. 2006. Control of phospholipid synthesis by phosphorylation of the yeast lipin Pah1p/Smp2p Mg2+-dependent phosphatidate phosphatase. *J. Biol. Chem.* 281:34537–34548. doi:10.1074/jbc.M606654200

Prinz, W.A., L. Grzyb, M. Veenhuis, J.A. Kahana, P.A. Silver, and T.A. Rapoport. 2000. Mutants affecting the structure of the cortical endoplasmic reticulum in *Saccharomyces cerevisiae*. *J. Cell Biol.* 150:461–474. doi:10.1083/jcb.150.3.461

Puhka, M., H. Vihinen, M. Joensuu, and E. Jokitalo. 2007. Endoplasmic reticulum remains continuous and undergoes sheet-to-tubule transformation during cell division in mammalian cells. *J. Cell Biol.* 179:895–909. doi:10.1083/jcb.200705112

Reimold, A.M., A. Etkin, I. Clauss, A. Perkins, D.S. Friend, J. Zhang, H.F. Horton, A. Scott, S.H. Orkin, M.C. Byrne, et al. 2000. An essential role in liver development for transcription factor XBP-1. *Genes Dev.* 14:152–157.

Reimold, A.M., N.N. Iwakoshi, J. Manis, P. Vallabhajosyula, E. Szomolanyi-Tsuda, E.M. Gravallese, D. Friend, M.J. Grusby, F. Alt, and L.H. Glimcher. 2001. Plasma cell differentiation requires the transcription factor XBP-1. *Nature.* 412:300–307. doi:10.1038/35085509

Ron, D., and P. Walter. 2007. Signal integration in the endoplasmic reticulum unfolded protein response. *Nat. Rev. Mol. Cell Biol.* 8:519–529. doi:10.1038/nrm2199

Sardiello, M., M. Palmieri, A. di Ronza, D.L. Medina, M. Valenza, V.A. Gennarino, C. Di Malta, F. Donaudy, V. Embrione, R.S. Polishchuk, et al. 2009. A gene network regulating lysosomal biogenesis and function. *Science.* 325:473–477.

Schwank, S., R. Ebbert, K. Rautenstrauss, E. Schweizer, and H.J. Schüller. 1995. Yeast transcriptional activator INO2 interacts as an Ino2p/Ino4p basic helix-loop-helix heteromeric complex with the inositol/choline-responsive

element necessary for expression of phospholipid biosynthetic genes in *Saccharomyces cerevisiae*. *Nucleic Acids Res.* 23:230–237. doi:10.1093/nar/23.2.230

Shaffer, A.L., M. Shapiro-Shelef, N.N. Iwakoshi, A.H. Lee, S.B. Qian, H. Zhao, X. Yu, L. Yang, B.K. Tan, A. Rosenwald, et al. 2004. XBP1, downstream of Blimp-1, expands the secretory apparatus and other organelles, and increases protein synthesis in plasma cell differentiation. *Immunity.* 21:81–93. doi:10.1016/j.immuni.2004.06.010

Shibata, Y., G.K. Voeltz, and T.A. Rapoport. 2006. Rough sheets and smooth tubules. *Cell.* 126:435–439. doi:10.1016/j.cell.2006.07.019

Shibata, Y., C. Voss, J.M. Rist, J. Hu, T.A. Rapoport, W.A. Prinz, and G.K. Voeltz. 2008. The reticulon and DP1/Yop1p proteins form immobile oligomers in the tubular endoplasmic reticulum. *J. Biol. Chem.* 283:18892–18904. doi:10.1074/jbc.M800986200

Snapp, E.L., R.S. Hegde, M. Francolini, F. Lombardo, S. Colombo, E. Pedrazzini, N. Borgese, and J. Lippincott-Schwartz. 2003. Formation of stacked ER cisternae by low affinity protein interactions. *J. Cell Biol.* 163:257–269. doi:10.1083/jcb.200306020

Sriburi, R., S. Jackowski, K. Mori, and J.W. Brewer. 2004. XBP1: a link between the unfolded protein response, lipid biosynthesis, and biogenesis of the endoplasmic reticulum. *J. Cell Biol.* 167:35–41. doi:10.1083/jcb.200406136

Sriburi, R., H. Bommiasamy, G.L. Buldak, G.R. Robbins, M. Frank, S. Jackowski, and J.W. Brewer. 2007. Coordinate regulation of phospholipid biosynthesis and secretory pathway gene expression in XBP-1(S)-induced endoplasmic reticulum biogenesis. *J. Biol. Chem.* 282:7024–7034. doi:10.1074/jbc.M609490200

Stuurman, N., N. Amodaj, and R.D. Vale. 2007. Micro-Manager: Open Source software for light microscope imaging. *Microscopy Today.* 15:42–43.

Takewaka, T., T. Zimmer, A. Hirata, A. Ohta, and M. Takagi. 1999. Null mutation in IRE1 gene inhibits overproduction of microsomal cytochrome P450Alk1 (CYP 52A3) and proliferation of the endoplasmic reticulum in *Saccharomyces cerevisiae*. *J. Biochem.* 125:507–514.

Travers, K.J., C.K. Patil, L. Wodicka, D.J. Lockhart, J.S. Weissman, and P. Walter. 2000. Functional and genomic analyses reveal an essential coordination between the unfolded protein response and ER-associated degradation. *Cell.* 101:249–258. doi:10.1016/S0092-8674(00)80835-1

Tyson, J.R., and C.J. Stirling. 2000. LHS1 and SIL1 provide a lumenal function that is essential for protein translocation into the endoplasmic reticulum. *EMBO J.* 19:6440–6452. doi:10.1093/emboj/19.23.6440

Urano, F., X. Wang, A. Bertolotti, Y. Zhang, P. Chung, H.P. Harding, and D. Ron. 2000. Coupling of stress in the ER to activation of JNK protein kinases by transmembrane protein kinase IRE1. *Science.* 287:664–666. doi:10.1126/science.287.5453.664

van Anken, E., E.P. Romijn, C. Maggioni, A. Mezghrani, R. Sitia, I. Braakman, and A.J. Heck. 2003. Sequential waves of functionally related proteins are expressed when B cells prepare for antibody secretion. *Immunity.* 18:243–253. doi:10.1016/S1074-7613(03)00024-4

Vembar, S.S., and J.L. Brodsky. 2008. One step at a time: endoplasmic reticulum-associated degradation. *Nat. Rev. Mol. Cell Biol.* 9:944–957. doi:10.1038/nrm2546

Voeltz, G.K., M.M. Rolls, and T.A. Rapoport. 2002. Structural organization of the endoplasmic reticulum. *EMBO Rep.* 3:944–950. doi:10.1093/embo-reports/kvf202

Voeltz, G.K., W.A. Prinz, Y. Shibata, J.M. Rist, and T.A. Rapoport. 2006. A class of membrane proteins shaping the tubular endoplasmic reticulum. *Cell.* 124:573–586. doi:10.1016/j.cell.2005.11.047

Webster, M., K.L. Witkin, and O. Cohen-Fix. 2009. Sizing up the nucleus: nuclear shape, size and nuclear-envelope assembly. *J. Cell Sci.* 122:1477–1486. doi:10.1242/jcs.037333

Wiest, D.L., J.K. Burkhardt, S. Hester, M. Hortsch, D.I. Meyer, and Y. Argon. 1990. Membrane biogenesis during B cell differentiation: most endoplasmic reticulum proteins are expressed coordinately. *J. Cell Biol.* 110:1501–1511. doi:10.1083/jcb.110.5.1501

Wright, R., M. Basson, L. D'Ari, and J. Rine. 1988. Increased amounts of HMG-CoA reductase induce "karmellae": a proliferation of stacked membrane pairs surrounding the yeast nucleus. *J. Cell Biol.* 107:101–114. doi:10.1083/jcb.107.1.101

Published

Supplemental material

JCB

Schuck et al., http://www.jcb.org/cgi/content/full/jcb.200907074/DC1

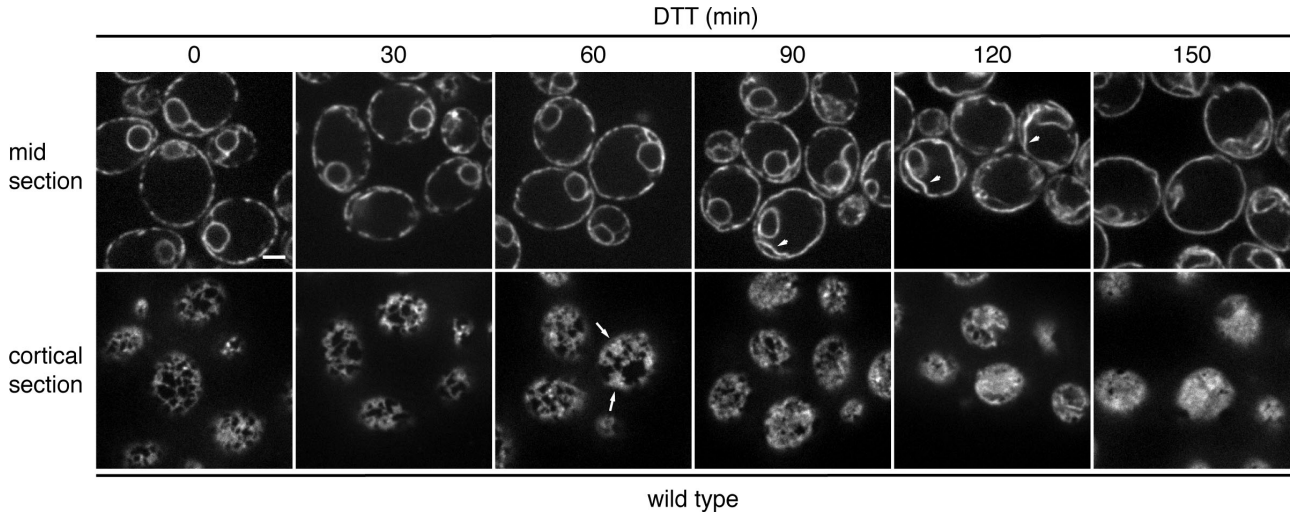

Figure S1. **Time course of ER membrane expansion induced by ER stress.** Sec63-GFP cells (SSY139) treated with DTT for up to 150 min. Representative cells from each time point are shown. ER expansion is clearly visible after 60 min and manifests itself in the increasingly frequent appearance of large membrane sheets in the peripheral ER (arrows) and later in the generation of extensions of the peripheral ER into the cytoplasm (arrowheads). Bar, 2 µm.

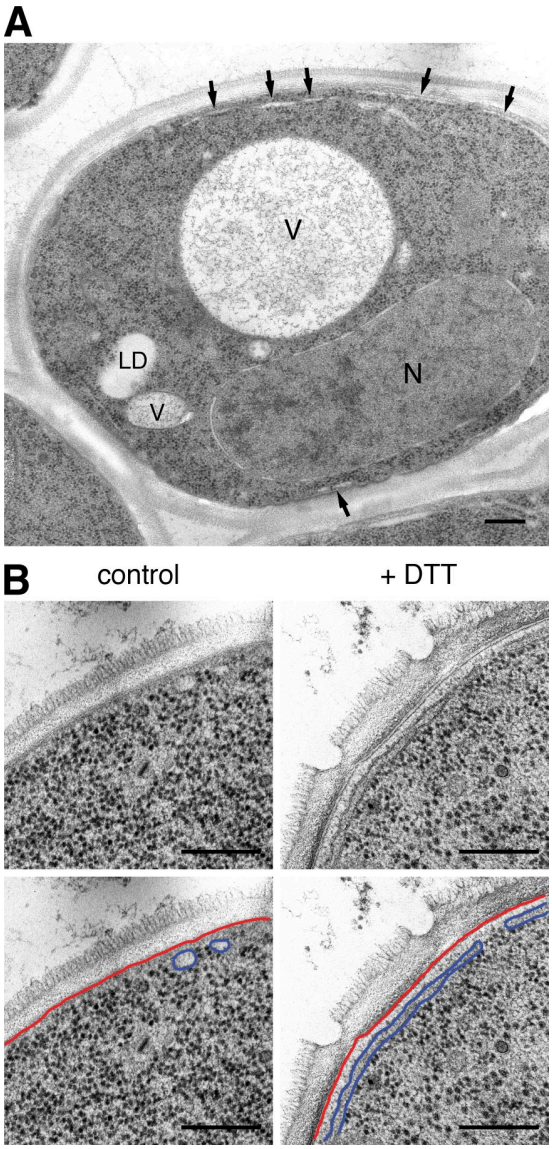

Figure S2. **Expansion of the peripheral ER induced by ER stress.** (A) Low magnification electron micrograph of untreated wild-type cells (SSY139). The peripheral ER (arrows) is visible underneath some areas of the plasma membrane. The vacuole usually appears black, but it is white in this particular image. This unexplained variation has been described previously (McDonald and Müller-Reichert, 2002). (B) High magnification electron micrographs of wild-type cells (SSY139) untreated (left) or treated with DTT for 2 h (right), illustrating the expansion of the peripheral ER during ER stress. (bottom) The peripheral ER is traced in blue, and the plasma membrane is in red. LD, lipid droplet; N, nucleus; V, vacuole. Bars, 250 nm.

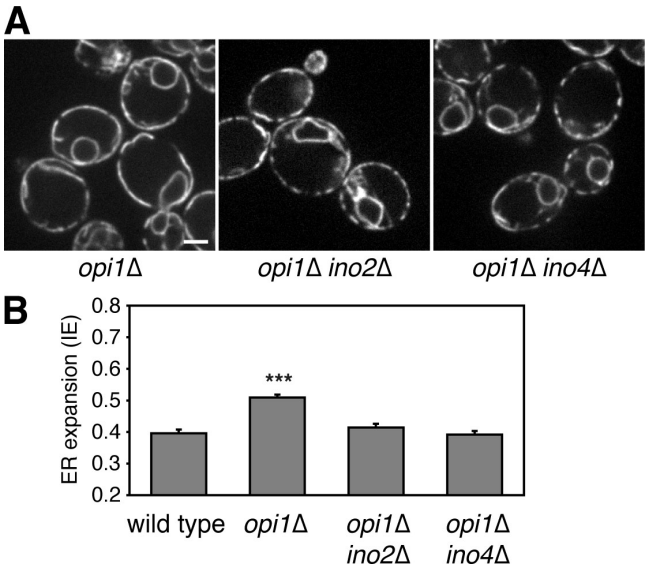

Figure S3. **Constitutive ER membrane expansion in *opi1* mutants requires *INO2* and *INO4*.** (A) Untreated *opi1*Δ, *opi1*Δ *ino2*Δ, and *opi1*Δ *ino4*Δ cells expressing Sec63-GFP (SSY290, SSY372, and SSY479). (B) Quantification of ER expansion from images obtained as in A. Statistical significance compared with wild-type cells of $P \leq 10^{-6}$ (***) is shown. Error bars indicate SEM. Bar, 2 µm.

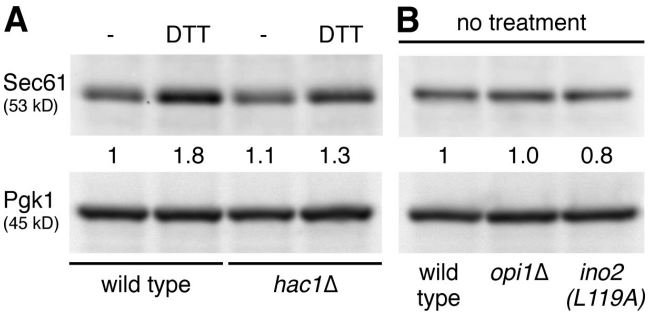

Figure S4. ***opi1* mutants and cells expressing ino2(L119A) have normal Sec61 protein levels.** (A) Western blot of Sec61 from wild-type (SSY139) and *hac1Δ* cells (SSY161) untreated or treated with DTT for 3 h. (B) Western blot of Sec61 from wild-type, *opi1Δ*, and *ino2(L119A)* cells (SSY433, SSY290, and SSY400). Pgk1 served as a loading control. Numbers indicate Sec61 protein levels compared with untreated wild-type cells and normalized to Pgk1.

Table S1. **Yeast strains used in this study**

Strain	Relevant genotype
SSY477	*Opi3-HA::HIS3*
SSY485	*Opi3-HA::HIS3 hac1::kan*
SSY484	*Opi3-HA::HIS3 ino2::kan*
SSY523	*RTN1-GFP::TRP1 dsRED-HDEL*
SSY531	*RTN1-GFP::TRP1 dsRED-HDEL opi1::kan* YEplac195
SSY532	*RTN1-GFP::TRP1 dsRED-HDEL opi1::kan* YEplac195-RTN1
SSY421	*SEC63-GFP::HIS3 RTN1-cherry::TRP1*
SSY429	*SEC63-GFP::HIS3 RTN1-cherry::TRP1 hac1::kan*
SSY473	*SEC63-GFP::HIS3 RTN1-cherry::TRP1 ino2::kan* pRS415-MET-ino2(L119A)
SSY478	*SEC63-GFP::HIS3 RTN1-cherry::TRP1 opi1::kan*
SSY139	*SEC63-GFP::HIS3 VPH1-cherry::TRP1*
SSY433	*SEC63-GFP::HIS3 VPH1-cherry::TRP1* pRS415-MET
SSY510	*SEC63-GFP::HIS3 VPH1-cherry::TRP1* YEplac195
SSY161	*SEC63-GFP::HIS3 VPH1-cherry::TRP1 hac1::LEU2*
SSY533	*SEC63-GFP::HIS3 VPH1-cherry::TRP1 hac1::LEU2* YEplac195
SSY434	*SEC63-GFP::HIS3 VPH1-cherry::TRP1 hac1::URA3* pRS415-MET
SSY430	*SEC63-GFP::HIS3 VPH1-cherry::TRP1 hac1::URA3 ino2::kan*
SSY439	*SEC63-GFP::HIS3 VPH1-cherry::TRP1 hac1::URA3 ino2::kan* pRS415-MET-INO2
SSY441	*SEC63-GFP::HIS3 VPH1-cherry::TRP1 hac1::URA3 ino2::kan* pRS415-MET-ino2(L119A)
SSY364	*SEC63-GFP::HIS3 VPH1-cherry::TRP1 hac1::kan opi1::LEU2*
SSY535	*SEC63-GFP::HIS3 VPH1-cherry::TRP1 hac1::kan opi1::LEU2* YEplac195
SSY536	*SEC63-GFP::HIS3 VPH1-cherry::TRP1 hac1::kan opi1::LEU2* YEplac195-RTN1
SSY369	*SEC63-GFP::HIS3 VPH1-cherry::TRP1 ino2::kan*
SSY400	*SEC63-GFP::HIS3 VPH1-cherry::TRP1 ino2::kan* pRS415-MET-ino2(L119A)
SSY460	*SEC63-GFP::HIS3 VPH1-cherry::TRP1 ino4::kan*
SSY467	*SEC63-GFP::HIS3 VPH1-cherry::TRP1 ire1::kan*
SSY290	*SEC63-GFP::HIS3 VPH1-cherry::TRP1 opi1::LEU2*
SSY372	*SEC63-GFP::HIS3 VPH1-cherry::TRP1 opi1::LEU2 ino2::kan*
SSY479	*SEC63-GFP::HIS3 VPH1-cherry::TRP1 opi1::LEU2 ino4::kan*

References

McDonald, K., and T. Müller-Reichert. 2002. Cryomethods for thin section electron microscopy. *Methods Enzymol.* 351:96–123.